A broadband CPW-fed T-shaped antenna for wireless communications

R.B. Hwang

Abstract: A novel broadband, dual-polarised coplanar-waveguide-fed T-shaped uniplanar antenna is presented. The raidation mechanism of such an antenna has been investigated, based on a full-wave numerical analysis and experimental measurement. In addition, the equivalent transmission line model incorporated with lumped-circuit elements is also presented to account for its radiation characteristics. Its performance has also been evaluated by integrating a 4-element CPW-fed T-shaped uniplanar antenna array with a simple beam forming network – a 4×4 Butler matrix. Its compact, low cost, easy-to-fabricate features together with good radiation characteristics are promising for application in wireless communication systems.

1 Introduction

Printed antennas with coplanar waveguide (CPW) feeds have attracted attention for many years. When compared with other printed radiating elements, CPW-fed antennas possesses advantages of not only a broad bandwidth, but also a smaller mutual coupling between adjacent lines and easier integration capability with solid-state active devices. In response to the increasing demand for compact, broadband and easily fabricated antennas for use in various wireless communication systems, several CPW-fed printed antennas have been developed over the past decade [1–8].

This paper presents a newly developed CPW-fed T-shaped uniplanar antenna printed on the commonly used Fr-4 epoxy substrate with relative dielectric constant 4.4 around 2 GHz. Unlike the previously published antenna structures, this structure is characterised by the single substrate, uniplanar configuration, compact size, does not require other matching network, and has no bonding wire connecting the ground planes. Also, due to the uniplanar configuration of this antenna, no parallel-plate waveguide mode will be excited, so the metallisation vias are not needed in our design. This facilitates the easy fabrication of this type of antenna.

In addition to the proposed structural parameters and the performace of the CPW-fed T-shaped uniplanar antenna, the radiation mechanism is investigated with the aid of the commerical software Ansoft HFSS based on the finite element method. The equivalent circuit model for figuring out the input impedance of the antenna is also established, treating the whole structure as the cascade of the equivalent transmission line for both the CPW-fed section and two shunted symmetrical/asymmetrical double-strip coplanar waveguide stubs. Lumped circuit parameters are also incorporated into the equivalent transmission lines in order to account for the resonance effect; for example, inductance introduced by the surface current and the capacitance resulting from the total electric field distribution on the wider slots. It is noted that the electric circuit model, i.e. equivalent transmission line network incorporated with lumped circuit elements, was proposed to give a physical insight into the behaviour of the antenna. It is useful for understanding the basic radiation phenomena of this antenna rather than design this type of antenna.

2 Antenna topology

The configuration of the proposed CPW-fed T-shaped uniplanar antenna is illustrated in Fig. 1*a*. The antenna is fabricated on a FR4 expoxy substrate 1.54 mm thick, with relative dielectric constant 4.4. The centre stripline of the CPW extends toward the rectangular metal patch through a short strip called the transition region. Hence the T-shaped uniplanar antenna is named after its geometric shape.

At the early stage of developing this antenna, the initial idea was to unfold a cylindrical dipole/monopole, print on a single substrate and then feed it with a coplanar waveguide. The original idea led to the prototype of the antenna illustrated in Fig. 1*b* and is named as the CPW-fed uniplanar monopole antenna [9]. The CPW-fed T-shaped uniplanar antenna evolved from the prototype through increased understanding and more insight into its radiation mechanism.

The size of the proposed antenna, including the CPW-fed section, is 0.4λ high and 0.22λ wide, where λ is the free-space wavelength at the design centre frequency, 2.4 GHz (its exact dimensions are shown in the Figures). The length of the CPW feed is typically about $0.5\lambda_g$, where λ_g is the guided-wave wavelength of the CPW at 2.4 GHz. Consequently, it is inevitable that when measuring the total length of the antenna, one cannot exclude the CPW-fed section since, as will be become clear latter on, the coplanar waveguide takes an important role in the radiation characteristics of the lower resonant frequency band.

3 Numerical simulation for the CPW-fed T-shaped uniplanar antenna

As illustrated in Fig. 1*a*, there are many structural parameters that determine the overall performance of the

IEE Proceedings online no. 20045016

doi:10.1049/ip-map:20045016

Paper received 6th May 2004. Originally published online: 26th October 2004

The author is with the Department of Communication Engineering, National Chiao Tung University, Hinchu, Taiwan, R.O.C

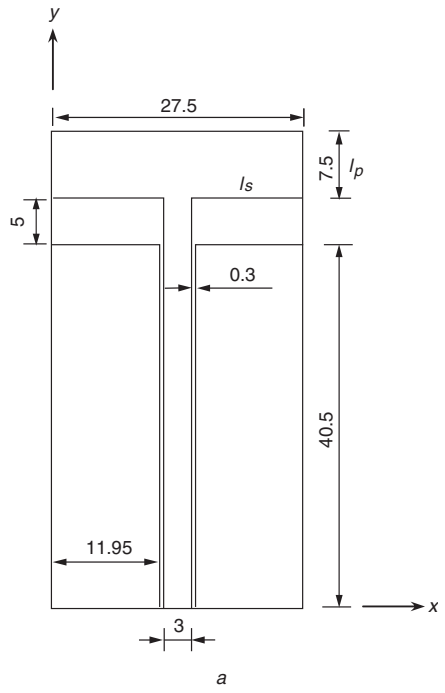

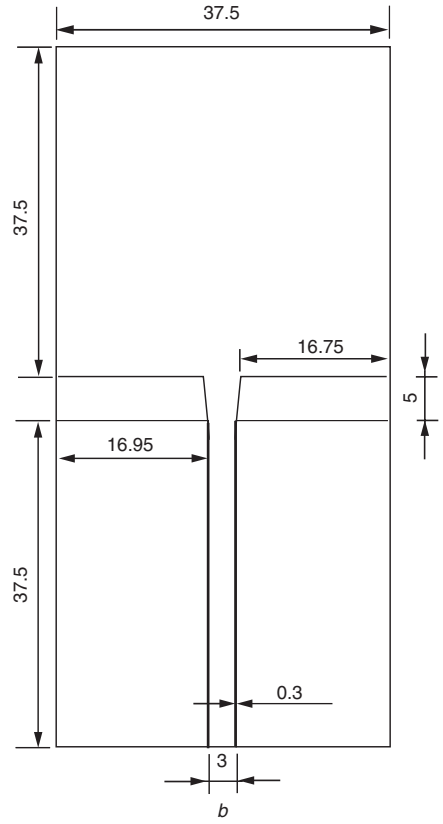

Fig. 1 *Configuration of CPW-fed uniplanar antenna (units in mm)*
a Proposed
b Prototype

antenna. Besides the well-known parameters which determine the characteristic impedance of a coplanar waveguide, the contribution and the influence of other parameters to the characteristics of the antenna are studied in this research.

In analysizing the CPW-fed T-shaped uniplanar antenna, Ansoft HFSS™ was employed to conduct a numerical simulation. Good agreements for predicting the two resonance frequencies can be observed between the simulated and measured reflection coefficient (S_{11}) for the

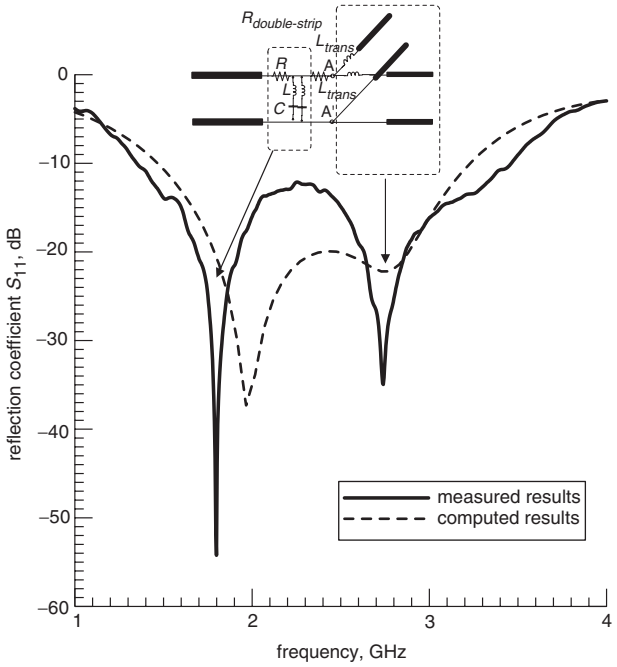

Fig. 2 *Measured and computed reflection coefficient (S_{11}) against frequency*

prototype configuration illustrated in Fig. 2. The magnitudes of these x- and y-direction magnetic fields (H_x and H_y) along several fixed x and y lines were then investigated for the further understanding of the radiation source, including both the electric and magnetic currents on this antenna.

By $\mathbf{J}_s = \hat{\mathbf{n}} \times \mathbf{H}$, the electric surface current density on the surface of metallic regions is mainly determined by H_x and H_y and has nothing to do with H_z. Therefore, H_x and H_y are plotted separately along several fixed x and y axes (i.e. at $x = 0$, 1.45, 1.85, 14.0 mm and $y = 18.75$, 36.5, 40.0, 43.5, 49.0 mm) for the prototype configuation. Figures 3 and 4 are the computed results. From these two Figures, it can be seen that H_x, which implies the y-direction surface current density J_y, is very large at the edges of both the CPW and the transition region. Also, H_x on the CPW-fed section dominates the resonant length of J_y and decays rapidly when flowing into the rectangular metal patch region. In another aspect, J_y flowing on the path consisting of the centre strip, the transition region and the metal patch, always has its counterpart with a smaller magnitude flowing in the opposite direction on the ground plane. On the other hand, due to the continuity of current, J_x approaches zero at the edge of the metal strip on ground planes or the centre conductor of the CPW. Besides, J_x (i.e. H_y) in the neighbourhood of the gaps decays monotonously from the centre line to both sides of the patch and always flows in the opposite direction. Since J_x is, in general, very small when compared with J_y, this implies that the y-direction surface current mainly determines the azmuthal radiation pattern of such an antenna.

In a word, the magnetic and electric current densities shown in Figs. 3, 4 and 5 are employed to demonstrate that the y-direction electric current concentrates in the edge of the metal strip or patch and thus determines the effective antenna length for radiating. However, the magnetic current distributed on the slot of double-strip coplanar waveguide shows that the x direction component is the major radiation source.

Except for the investigation of the magnetic field distribution on the antenna, the electric field distributions

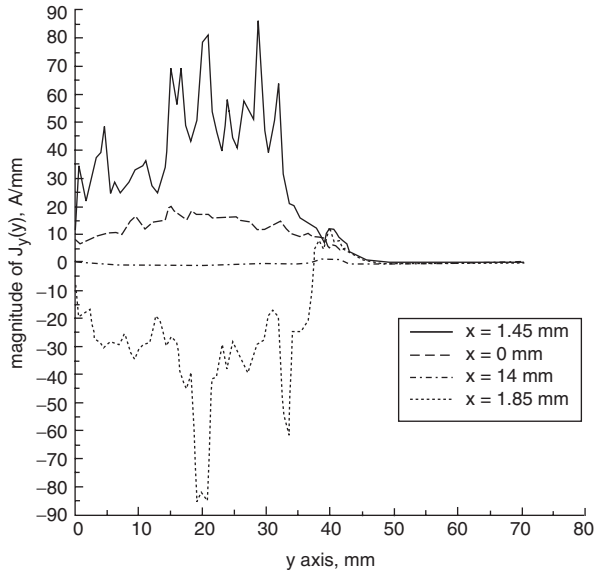

Fig. 3 *Magnitude of $\boldsymbol{H}_x$ along certain x-line cuts*

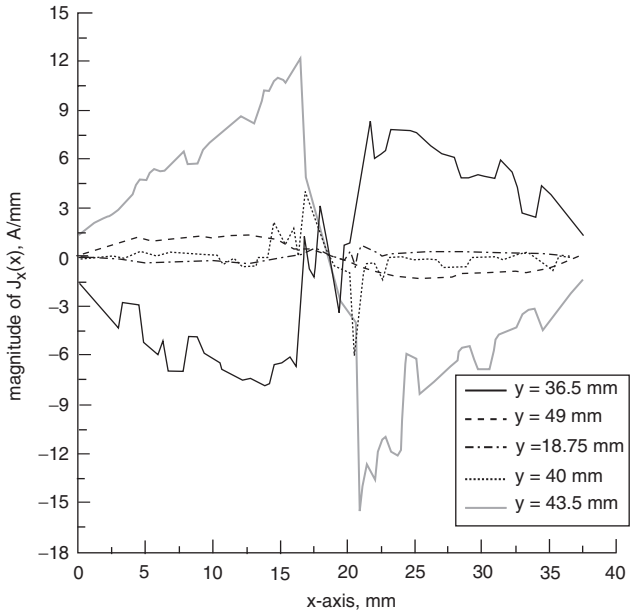

Fig. 4 *Magnitude of $\boldsymbol{H}_y$ along certain y-line cuts*

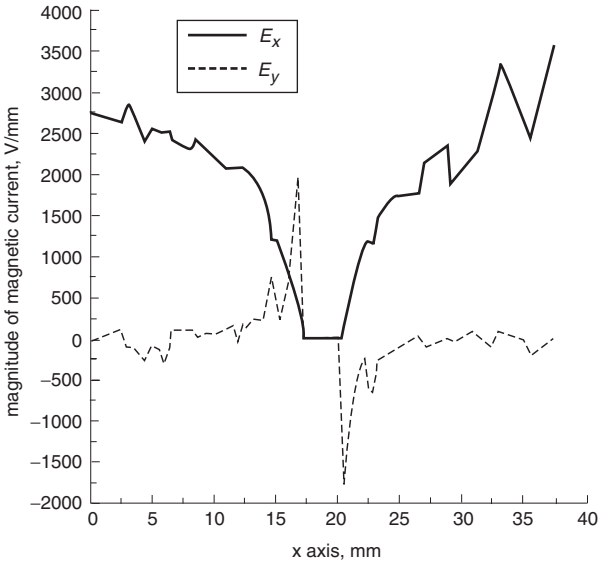

Fig. 5 *Magnitudes of $\boldsymbol{E}_x$ and $\boldsymbol{E}_y$ along the gaps between double-strip coplanar waveguides*

must be clearly examined since they constitute the magnetic currents density on the gaps between the double-strip coplanar waveguides. Figure 5 shows both the E_x and E_y distributions along the gaps (i.e. at $y = 40.5$ mm line). It shows that at both sides of the transition region, the y-direction magnetic current M_y always flows in the opposite direction, while M_x always flows in the same direction. In addition, the magnitude of E_y along the gaps is much higher than that of H_y in the region of the gap edges. Therefore, it may be inferred that the magnetic currents flowing along the lateral (x) direction and the electric current along the longitudinal (y) direction are the two main radiating sources of this kind of antenna. This explains why the antenna possesses a relatively high cross-polarisation level for both azimuth and elevation radiation patterns.

4 Establishment of the equivalent circuit model

As described in the previous Section, the establishment of the electric circuit model was to facilitate physical insight into this antenna instead of obtaining engineering design parameters. It is useful for parameteric study not to design the antenna; what occurs to the input impedance of this antenna can be known from the electric circuit model. For instance, what happens to the two resonance frequencies if the slots of the double-strip CPW are changed. As for the empirical rules of these lumped circuit elements, they are closed, related to the field problem which requires complicated mathematical process. They are important, but beyond the scope of this paper and remain to be studied in detail in the future.

The short strip which connects the centre stripline of the coplanar waveguide and the upper rectangular metal strip, in reality, affords the structural transition from uniform CPW to two double-strip CPWs. In light of this observation and inference, the structural parameters which dominate the resonant frequency, impedance matching and in turn its reflection coefficient are determined by the transition region as well as the length (l_s), slot width (s), and ground plane width ($w1$ and/or $w2$) of the double-strip coplanar waveguide.

According to the numerical simulation, it is known that the surface electric current density is flowing primarily along the longitudinal (i.e. y) direction while the magnetic currents on the two gaps of the double-strip CPWs are produced mainly in the lateral (i.e. x) direction. Thus when constructing the equivalent circuit model, the aim was to separate the two orthogonal radiation sources and sketch the circuit model on the basis of their physical properties.

Figure 6 illustrates the equivalent transmission line model incorporated with the lumped circuit elements of the CPW-fed T-shaped uniplanar antenna. They will be discussed in detail in the rest of this Section. As described above the whole antenna structure can be treated as one CPW-fed section being 'transformed' into two double-strip coplanar waveguides through the aid of the short strip. This consideration corresponds to the two open transmission line stubs representing the double-strip coplanar waveguides connected in parallel with the rest of the equivalent circuit. The characteristic impedance of the symmetrical/asymmetrical double-strip coplanar waveguide with finite substrate thickness is given in [10]. For the symmetrical double-strip coplanar waveguide with strip width w and separation s on a substrate of relative permittivity ε_r and thickness h, the characteristic impedance for zero conductor thickness is

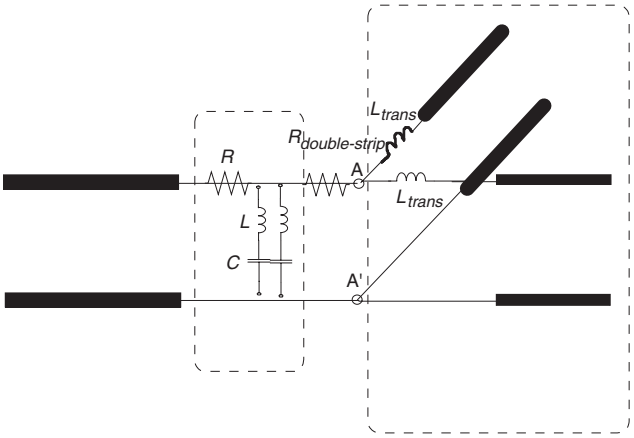

Fig. 6 *Equivalent transmission line model incorporated with lumped-circuit elements for CPW-fed uniplanar*

given below

$$Z_0 = \eta_0 K(k)/\{\sqrt{\varepsilon_{r,eff}} K(k')\} \tag{1a}$$

$$k = s/(s + 2w) \tag{1b}$$

$$k' = \sqrt{1 + k^2} = \sqrt{1 - (s/d)^2} \tag{1c}$$

where $K(k)$ is the complete elliptical integral of first order with modulus k, or with the complementary modulus k', and $\varepsilon_{r,eff}$ is the effective dielectric constant of the structure. As for the asymmetrical case, which is mainly characterised by two strip transmission lines of width $w1$ and $w2$, the characteristic impedance becomes

$$Z_0 = \eta_0 K(k)/\{2\sqrt{\varepsilon_{r,eff}} K(k')\} \tag{2a}$$

$$k = \sqrt{1 - \frac{1}{\{1 + (s + w1)\}\{1 + (s/w2)\}}} \tag{2b}$$

$$k' = \sqrt{1 - k^2} = \sqrt{w1w2/(w1 + s)(w2 + s)} \tag{2c}$$

All the remaining equations required for calculating the characteristic impedance and the effective dielectric constant of either case can refer to [10] and they are neglected for the sake of brevity in this paper.

With the double-strip coplanar waveguides introduced in the equivalent circuit model, it was recognised that the widths of the two strips were actually the length of the CPW-fed section and the height of the upper rectangular metal strip (l_p), respectively. In other words, for a fixed lateral dimension of the antenna (i.e. a fixed length of the two double-strip coplanar waveguides), the variation in either the length of the CPW-fed section or the height of the upper rectangular metal strip actually changes the characteristic impedance of the double-strip coplanar waveguide. This would further alter the input impedance of this antenna. Hence it is straightforward to write down the input impedance seen from the nodes A and A' looking into the two shunt double-strip CPWs.

Because the lossless transmission line is assumed in calculating the input impedance of the open double-strip CPWs, a lumped-element resistance $R_{double\text{-}strip}$ is added in series to them. $R_{double\text{-}strip}$ is employed to model the conductor and dielectric losses for the double-strip CPWs. In the case study proposed in this paper, the approximate value is about 11–13 Ω.

In addition to the series resistance $R_{double\text{-}strip}$, two lumped-element inductors L_{trans} account for the inductance property produced by the high surface current density flowing along the two edges of the transition region. They are individually connected in series with their corresponding open transmission line stub. To estimate its approximate value, the emperical rule estimating the unit length inductance, $L \cong 10$ nH/inch was employed. Therefore, the inductance value would be linearly proportional to the length of the transition region.

From the circuit theory point of view, the above-mentioned two open transmission line stubs together with the series lumped-element inductance and resistance will constitute a series resonant circuit. This may corresponds to one of the resonant frequencies in Fig. 2. To demonstrate this consideration, the lengths of both the transition region and the double-strip CPWs were fixed and the total longitudinal length of the overall structure was varied. The results, though not shown, agree very well with the reasoning. When compared with the variation in the domain of cotangent function (i.e. $k_0\sqrt{\varepsilon_{r,eff}} l_s$), the changes in the characteristic impedance of the double-strip CPW for different strip width combinations ($w1$ and $w2$) is negligibly small. This explains why the higher resonant frequency remains almost unchanged as the total length of the antenna changes significantly. Thus the higher resonant frequency band can be ascribed to the two shunt open-circuited double-strip CPWs connected in series with their individual inductance L_{trans}.

It is also interesting to note that the lower resonant frequency band does change significantly, both in the level of S_{11} and in the resonant centre frequency, with the variation of the total length of the antenna. This further leads to the electromagnetic properties associated with the surface current flowing along the longitudinal direction of the antenna in the equivalent circuit model being taken into account.

As illustrated in Fig. 6, L is responsible for the inductance effect produced by the current flowing along the edges of the upper rectangular metal patch/strip. In accordance with the well-known understanding and also the numerical simulation, the surface current density at the edges is much higher than that in any other regions of the antenna. Accordingly, the inductance value is approximated by applying the emperical rule described above for both the prototype patch structure ($l_s = 16.95$ mm, $l_p = 37.5$ mm) and the T-shaped strip structure ($l_s = 11.95$ mm, $l_p = 7.5$ mm). It should be noted that the antenna length responsible for radiating is determined by measuring the path lengthing which the current flows to the position where the current decays to an insignificant value. For the prototype structure, the total path length is ($l_s + l_{yp}$), where l_{yp} denotes the y-directed path length before the current decays to nearly zero on the rectangular patch. Based on the full-wave simulation, l_{yp} is chosen to be about 17.5 mm in the equivalent circuit simulation. For the T-shaped structure, y-directed current is forced to zero due to the limitation on l_p. For this reason, it is certain that l_{yp} is equal to l_p.

The capacitance C models the discontinuity between the coplanar waveguide and the double-strip coplanar waveguide. Through the parameters extracted from the variation of return loss versus frequency, the value of $C \approx 0.58$ pF was obtain in the case studies. Because parts of the on-patch surface current return to two ground planes of the CPW feed by means of the displacement currents, two sets of reactance components composed of the above-mentioned inductance L and a series capacitance C are connected in parallel. Consequently, the lower resonant frequency band is due primarily to the electrical properties in the longitudinal direction.

The resistance R accounts for the real part of the impedance seen looking from the CPW feed end towards

the rest of the antenna structure. The introduction of it is to approximately tune the matching level of the whole structure to the standard 50 Ω system.

As previously described in this paper, the length of the CPW feed plays a significant role for both the level of S_{11} and the resonant frequency bands and it has been asserted that it should be $0.5\lambda_g$. This may be concluded from the conventional equation for computing the input impedance of a transmission line, the term $\tan(k_0\sqrt{\varepsilon_{eff}}\cdot l)$ vanished if l equals $0.5\lambda_g$. This results in the input impedance being exactly equal to the load impedance. Specifically, when this occurs, the resonant frequencies are mainly determined by the two sets of reactance components, for example $\{L, C\}$ and $\{L_{trans}$, open transmission line stubs$\}$.

The computed results on the basis of the equivalent circuit model and the measured data for both the prototype and the T-shaped uniplanar antenna are shown in Figs. 7 and 8. Good agreement between them can be observed which further ensures the validation and feasibility of the proposed circuit model for this kind of antenna.

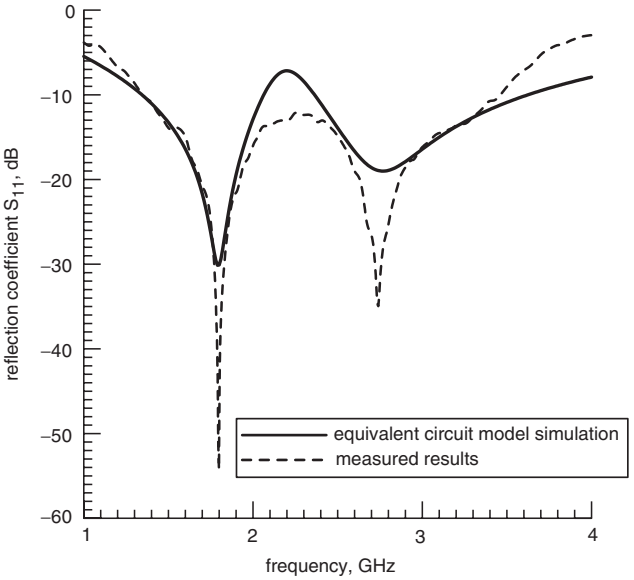

Fig. 7 *Measured and simulated reflection coefficient (S_{11}) obtained by equivalent circuit model for prototype structure shown in Fig. 1b*

5 Measurement results and radiation pattern

For the T-shaped structure, the bandwidth below −10dB is about 61.5% (from 2.205 GHz to 3.68 GHz), and about 88.3% (from 1.342 GHz to 3.46 GHz) for the prototype one, all computed with respect to the design centre frequency 2.4GHz.

The radiation patterns of the T-shaped structure are shown in Figs. 9 and 10. Due to lack of space, the radiation patterns of the prototype configuration are not shown here. Because both the magnetic and electric currents exist and, moreover, the electric currents do not purely flow in the same direction and along the same path, the radation patterns are not absolutely omnidirectional, especially for the elevation pattern.

6 Integration of the proposed antenna to the simple beam forming network – the Butler matrix

Recently, switched-beam antenna systems using different beam forming networks (BENs) or array antenna elements

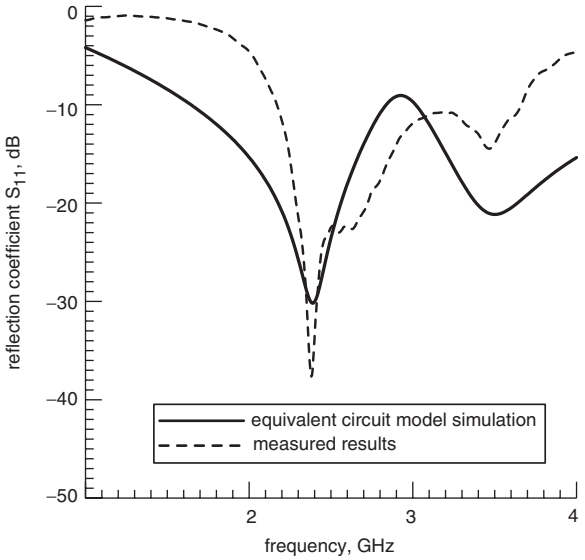

Fig. 8 *Measured and simulated reflection coefficient (S_{11}) obtained by equivalent circuit model for T-shaped structure shown in Fig. 1a*

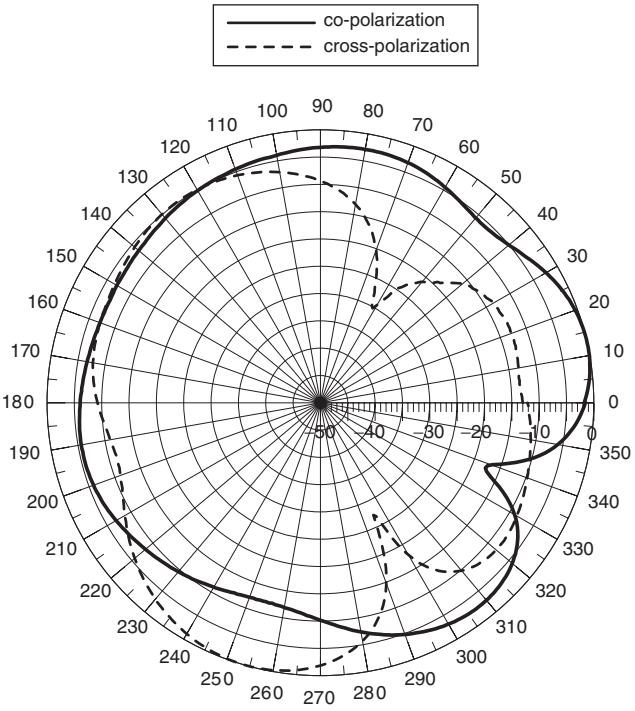

Fig. 9 *Azimuth radiation pattern of CPW-fed T-shaped uniplanar antenna illustrated in Fig. 1a*

have been proposed and verified in the literature [11]. However, these research works were mainly focused on the numerical simulation for the BFN, such as Butler matrix [11] and modified Butler matrix [12, 13], or the system performance evaluation of switched-beam antennas by using commonly used monopole- or patch- antennas, which suffer narrow bandwidth or power return loss.

To demonstrate the potential and feasibility of the proposed CPW-fed T-shaped uniplanar antenna in the application of wireless communications, a simple switched-beam antenna system was constructed by applying a conventional 4×4 Butler matrix as the phase shifting network. The structure and operation of the Butler matrix was proposed in detail by [11]. With the assumption of a negligibly small mutual coupling between the identical array elements, the far-zone field of the 4-element linear array can

be easily obtained by

$$E_{rad} = \left\{ \sum_{n=1}^{N} [A_n e^{j\alpha_n} e^{jk\hat{r}e_n}] \right\} \cdot \left[\frac{e^{-jkr}}{r} f(\theta, \phi) \right] \qquad (3)$$

where the first term in the form of the summation represents the array factor, which is determined by the signal amplitude (A_n), phase (α_n) of the beam forming network, as well as the position vector (r_n) of an individual array element. The second term is the far-field radiation pattern of a single separated array element.

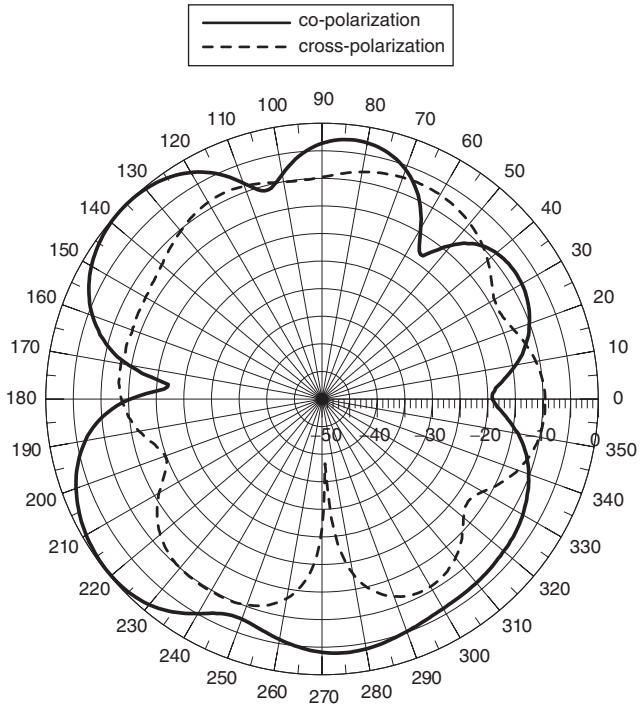

Fig. 10 *Elevation radiation pattern of CPW-fed T-shaped uniplanar antenna illustrated in Fig. 1a*

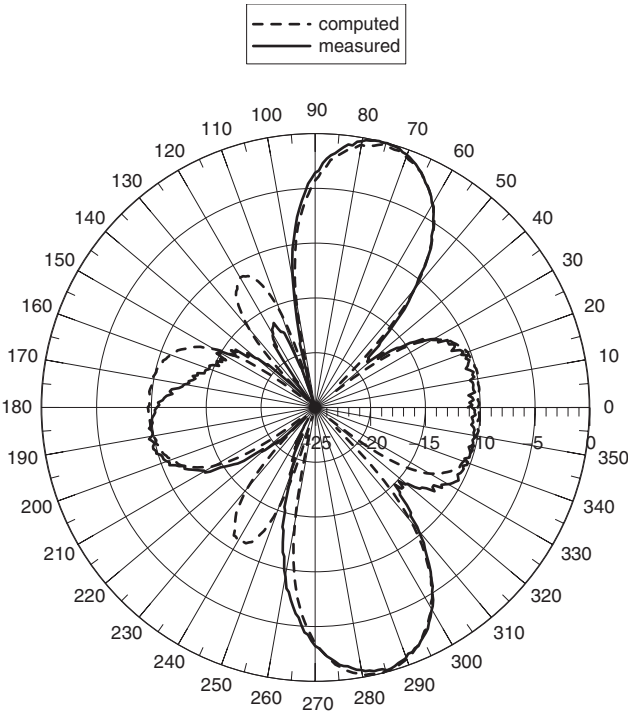

Fig. 11 *Azimuth radiation pattern of switched-beam antenna for port 1*

Figures 11–14 illustrate the measured and computed radiation patterns of individual input ports and are plotted in the format of solid and dashed lines, respectively. The computed result was obtained by multiplying the radiation pattern of an isolated array element (i.e. in the absence of another identical array element) with the array factor. Fairly good agreements between the measurements and isolated-element-based prediction are apparently observed in these Figures. It is noted that due to the non-significant mutual coupling among the array elements, the isolated element pattern is sufficient to predict the radiation patterns of the switched-beam antenna.

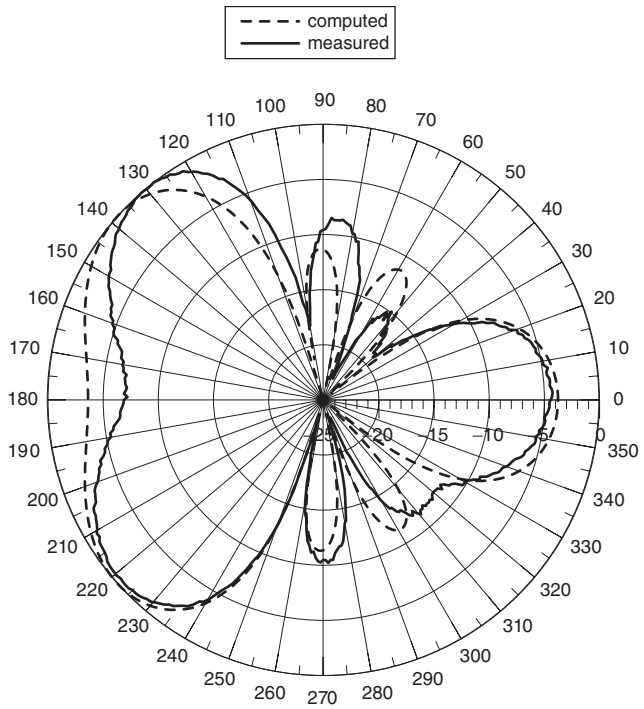

Fig. 12 *Azimuth radiation pattern of switched-beam antenna for port 2*

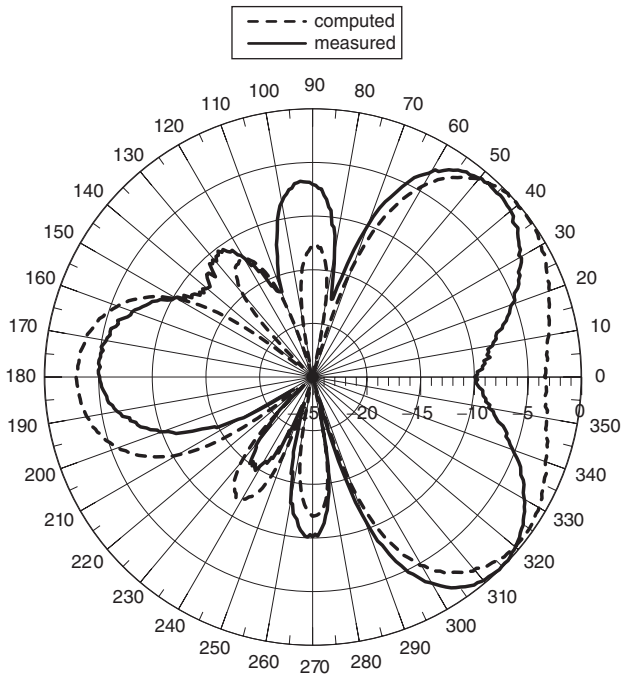

Fig. 13 *Azimuth radiation pattern of switched-beam antenna for port 3*

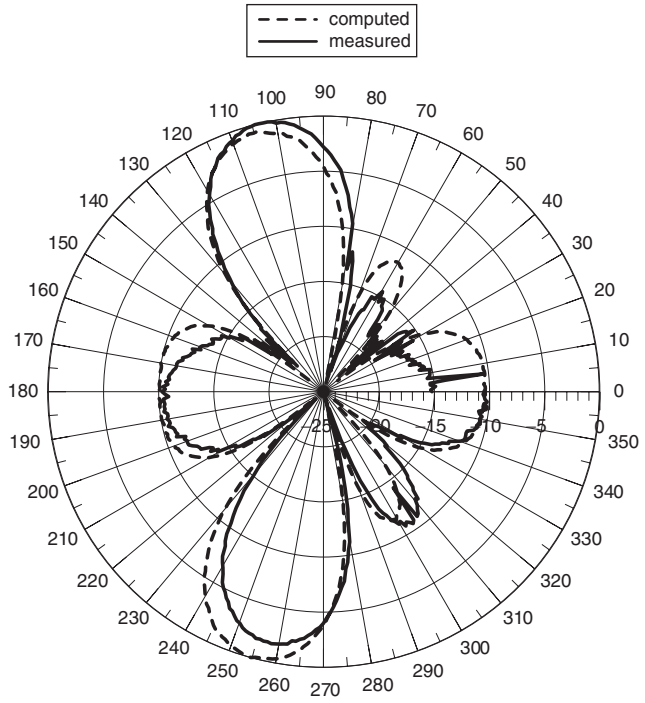

Fig. 14 *Azimuth radiation pattern of switched-beam antenna for port 4*

7 Conclusion

A novel broadband, dual-polarised CPW-fed T-shaped uniplanar antenna has been proposed. Such an antenna is a broadband design, featuring at least 61.5% operational bandwidth with respect to the design centre frequency. Except for the numerical analysis demonstrating the radiation mechanism due to two orthogonal radiation sources, including electric and magnetic currents, an equivalent transmission line model incorporated with lumped-circuit elements was established. The equivalent circuit model provided a physical insight to account for the input impedance of this kind of antenna.

8 Acknowledgement

This research is sponsored by the National Science Council under the contract number: NSC 93-2213-E009-154. The author would like to thank Prof. J. D. Tseng, National Chin Yi Institute of Technology, Taichun, Taiwan, R. O. C., for his help in carrying out numerical simulation using HFSS.

9 References

1 Tilley, K., Wu, X.-D., and Chang, K.: 'Coplanar waveguide fed coplanar strip dipole antenna', *Electron. Lett.*, 1994, **30**, (3), pp. 176–177
2 Kormanyos, B.K., Harokopus, W., Katehi, L.P.B., and Rebeiz, G.M.: 'CPW-fed active slot antennas', *IEEE Trans. Microw. Theory Tech.*, 1994, **42**, pp. 541–545
3 Liu, H.-C., Horng, T.-S., and Alexopoulos, N.G.: 'Radiation of printed antennas with a coplanar waveguide feed', *IEEE Trans. Antennas Propag.*, 1995, **43**, (10), pp. 1143–1148
4 Laheurte, J.-M., Katehi, L.P.B., and Rebeiz, G.M.: 'CPW-fed slot antennas on multilayer dielectric substrates', *IEEE Trans. Antennas Propag.*, 1996, **44**, (8), pp. 1102–1111
5 Johnson, J.M., and Rahmat-Samii, Y.: 'The tab monopole', *IEEE Trans. Antennas Propag.*, 1997, **45**, (1), pp. 187–188
6 Hettak, K., Delisle, G., and Boulmalf, M.: 'A novel integrated antenna for millimeter-wave personal communication systems', *IEEE Trans. Antennas Propag.*, 1998, **46**, (11), pp. 1757–1758
7 Litva, J., Wu, C., Bi, Z., and Wu, K.: 'Some consideration for microstrip coplanar-waveguide antennas'. IEEE APS Symp. Dig., 1992, pp. 491–494
8 Lin, Y.-D., and Tsai, S.-N.: 'Coplanar waveguide-fed uniplanar bow-tie antenna', *IEEE Trans. Antennas Propag.*, 1997, **45**, (2), pp. 305–306
9 Chang, Y.J., and Hwang, R.B.: 'Switched beam system for low-tier wireless communication systems'. Asia Pacific Microwave Conference, Taipei, Taiwan, 2001, Vol. 1, pp. 946–949
10 Hoffmann, R.K.: 'Handbook of microwave integrated circuits' (Artech House, 1987)
11 Liberti, J.C., and Rappaport, J.T.S.: 'Smart antennas for wireless communications: IS-95 and third Generation CDMA applications' (Prentice Hall PTR, 1999)
12 Fu, K.K., and Lai, A.K.Y.: 'FDTD optimization of beam forming network for multibeam antenna'. IEEE Antennas and Propagation Society Int. Symp., 2002, Vol. 4, pp. 2028–2031
13 Feng, Z., and Yang, Y.: 'Multibeam plane array using modified Butler matrix circuits'. Asia Pacific Microwave Conf., Singapore, 1999, Vol. 1, pp. 103–106